Modeling Electrochemical Processes with Grand Canonical Treatment of Many-Body Perturbation Theory

Ziyang Wei,[†] Florian Göltl,[‡] Stephan N. Steinmann,[*,¶] and Philippe Sautet[*,†,§]

[†]*Department of Chemistry and Biochemistry, University of California, Los Angeles, California, 90095, United States*

[‡]*Department of Biosystems Engineering, The University of Arizona, Tucson, Arizona, 85721, United States*

[¶]*ENS de Lyon, CNRS UMR 5182, Laboratoire de Chimie, 46 Allée d'Italie, 69342 Lyon, France*

[§]*Department of Chemical and Biomolecular Engineering, University of California, Los Angeles, California, 90095, United States*

E-mail: stephan.steinmann@ens-lyon.fr; sautet@ucla.edu

Abstract

Electrocatalysis plays a key role in sustainable energy conversion and storage. The grand canonical treatment of electrons, which accounts for the electrochemical potential explicitly, is critical to model at the atomic scale and understand these reactions at electrified interfaces. However, such a grand canonical treatment for electrocatalytic modeling is in practice restricted to a treatment of electronic structure with density functional theory and more accurate methods are in many cases desirable. Here, we develop an original workflow combining the grand canonical treatment of electrons with many-body perturbation theory in its random phase approximation (RPA). Using the

potential dependent adsorption of carbon monoxide on copper (100) facet, we show that the grand canonical RPA energetics provide the correct on-top Cu geometry for CO at reducing potential. The match with experimental results is significantly improved compared to the functionals at the generalized gradient approximation level, which is the most commonly used approximation for electrochemical applications. We expect this development to pave the way to further electrochemical applications using RPA.

Electrocatalysis is at the heart of various sustainable energy conversion and storage technologies,[1] such as water splitting,[2] fuel-cells,[3] and CO_2 conversion.[4,5] The electrochemical reactions involved in these processes, including carbon dioxide reduction reaction (CO_2RR), hydrogen evolution reaction (HER), oxygen reduction reaction (ORR), etc., happen at solid-liquid interfaces in the presence of an applied electric potential.[6] For the first principles based atomic scale modeling of such electrocatalytic processes, explicitly including the effects of the applied potential have been shown to be essential: the constant electrode potential (CEP) model is found to qualitatively change results and match better with experiments compared to the simpler constant charge model.[7–9] At the same time, the CEP model requires grand canonical density functional theory[10,11] (GC-DFT) calculations, i.e., explicitly changing the number of electrons to tune the electrode potential.[6,8,12,13] The non-equilibrium Green's function (NEGF) approach[14–17] which focuses on the quantum transport simulation, is an alternative approach for modeling electrified interfaces. However, to the best of our knowledge, NEGF has, so far, not been coupled to a description of the liquid electrolyte. Therefore, NEGF cannot, for the time being, capture realistic capacities of the interface, which are, however, crucial for the chemical reactivity as a function of the applied potential.

The aforementioned studies, however, are based on the DFT energies obtained at the generalized gradient approximation (GGA) level. GGA functionals are known to sometimes lead to qualitative and quantitative errors in the description of molecular adsorption. One important example of this shortcoming is the CO adsorption puzzle:[18–20] GGA functionals incorrectly predict the preference for adsorption in the face center cubic (FCC) site on the

(111) facets and the hollow site on the (100) facets instead of the experimentally determined adsorption in the on top position and overestimate the adsorption energy. The random phase approximation[21,22] (RPA), a post Hartree-Fock (HF) method based on the many-body perturbation theory,[23,24] has been shown to give a correct description of CO adsorption on various metal surfaces, including copper (Cu).[25,26] Additionally, the metal surface energies are described accurately using this method. These two aspects are essential to correctly describe the adsorption energies of adsorbates involved in CO_2RR.[27,28] Therefore, the combination of the grand canonical treatment with RPA energetics appears as an appealing solution to correctly describe both the molecule-surface interaction[29] and the potential effects. In the past it has been shown that several approaches[30–33] might improve specific surface properties compared to RPA. However, these approaches go beyond the scope of this work. To the best of the authors' knowledge, currently implementations of RPA using periodic boundary conditions are non-self-consistent. Hence the typical approach of grand canonical DFT treatment, which relies on the Fermi level obtained from self-consistent electronic structure calculations, cannot be directly applied.

In this work we develop an alternative approach, which is purely based on the system's energy and can be used to determine the Fermi level via a partial derivative of the energy with respect to the number of electrons. We show that at the DFT level, this approach is equivalent to using the Fermi level value obtained from self-consistent electronic structure calculations. We furthermore demonstrate how this energy based approach can be used to perform grand canonical RPA (GC-RPA) calculations. We then apply this method to the potential dependent adsorption of carbon monoxide (CO) on Cu(100), and show that GC-RPA calculations lead to a qualitatively different description of this process compared to results obtained at the GGA level of theory, performed using the Perdew-Burke-Ernzerhof[34] (PBE) and revised Perdew-Burke-Ernzerhof[35] (RPBE) functionals. These GC-RPA results match better with experimental evidences compared to GC-DFT and illustrate that the grand canonical treatment at the RPA level is a powerful tool to deepen our understanding

of interfacial electrochemical phenomena.

We briefly summarize the RPA energy formulas here, and more details, including the treatment of partial partial occupancy,[36,37] can be found in the literature.[23,24,36–40] The total RPA energy consists of the exact exchange (EXX) component, i.e., Hartree-Fock (HF) exchange, calculated for the occupied orbitals and the RPA correlation component based on both the occupied and unoccupied orbitals:

$$E^{RPA} = E^{EXX}([\psi_{occ}]) + E_c^{RPA}([\psi_{occ}, \psi_{uocc}]) \tag{1}$$

To apply the grand canonical treatment for electrochemical purposes, we need to account for the implicit solvation in the RPA framework. We account for the presence of solvation effects at the DFT level by computing orbitals combining the linearized Poisson-Boltzmann equation, as implemented by Hennig et al.[6,41] in VASP.[42] Starting from these orbitals ($\psi_{occ,solvation}, \psi_{uocc,solvation}$), we add the solvation energy based on the electron density, which is determined by the occupied orbitals, to the RPA total energy expression. The RPA energy, which incorporates implicit solvation effects, is then expressed as:

$$E_{sol}^{RPA} = E^{EXX}([\psi_{occ,solvation}]) + E_c^{RPA}([\psi_{occ,solvation}, \psi_{uocc,solvation}]) + E^{solvation}([\psi_{occ,solvation}]) \tag{2}$$

where the solvation energy $E^{solvation}([\psi_{occ,solvation}])$ is obtained in the non-self-consistent HF step and only depends on the charge density.

The details of GC-DFT can be found in the literature[6,13,43] and we summarize the most important procedures as follows. The net number of electrons, $n_{surface}$, is calculated as:

$$n_{surface} = N_{surface} - N_{surface,neutral} \tag{3}$$

where $N_{surface}$ is the number of electrons of the surface system and $N_{surface,neutral}$ is the number of electrons in the neutral, i.e., non-charged, state. The DFT energy for charged

states is, in this context, obtained as:

$$E_{surface} = E_{surface,raw} + \epsilon_{Fermi\ shift} n_{surface} \tag{4}$$

where $E_{surface,raw}$ is the "raw" energy printed by VASP and $\epsilon_{Fermi\ shift} n_{surface}$ is the necessary[6] correction term accounting for the difference ($\epsilon_{Fermi\ shift}$) in the reference energy of the electron between the "internal" reference level and vacuum. Then the grand canonical electronic energy of a surface model, $G(U_{vac})$, is obtained as:

$$G(U_{vac}) = E_{surface} - n_{surface}\mu_{electron} \tag{5}$$

where the chemical potential of an electron, is determined as:

$$\mu_{electron} = qU_{vac} = -eU_{vac} \tag{6}$$

where U_{vac} is the potential of the system with reference to the vacuum level and q is the charge of an electron. The potential of the system with reference to the vacuum can be determined using two components in the implementation of Hennig et al.:[6,41] the Fermi level (ϵ_F) with reference to the "internal" zero energy reference and the Fermi shift which is the difference between the "internal" energy reference and the vacuum level:

$$-eU_{vac} = \epsilon_F + \epsilon_{Fermi\ shift} \tag{7}$$

We call this the "SCF approach" herein. In the current implementation of RPA in periodic boundary conditions, the RPA energy is a single shot energy based on underlying DFT orbitals and one-electron energies. Therefore, the self-consistent electronic structure, and hence the self-consistent Fermi level, are not available. As a consequence, the "SCF approach", which uses ϵ_F in Eq. 7, cannot be directly applied at the non-self-consistent

RPA level. To circumvent this fundamental difficulty, we propose to use an alternative approach, which we call the "energetic" approach and does not require the self-consistent electronic structure. Combining Eq. 6 and Eq. 7 with the relationship of internal energy E and chemical potential μ in thermodynamics, we have:

$$\epsilon_F = \mu_{electron} - \epsilon_{Fermi\ shift} = \frac{\partial E_{surface}}{\partial n_{electron}} - \epsilon_{Fermi\ shift} = \frac{\partial E_{surface,raw}}{\partial n_{electron}} \tag{8}$$

After calculating a series of RPA energies with different number of electrons and performing a quadratic fitting of the $E(n_{surface})$ relationship,[6] the Fermi level values can be obtained analytically as a linear function of $n_{surface}$.

It is worth mentioning that for metallic systems the free electronic energy G in GC treatments exhibits a quadratic behavior around the potential of zero charge (PZC), U_0:

$$G(U) = G(U_0) - \frac{1}{2}C(U - U_0)^2 \tag{9}$$

where C is the capacitance of the model and the PZC, U_0, is the potential of the neutral, i.e., non-charged system. The PZC can be viewed as the work function of the solvated system as it describes the process of taking one electron from the Fermi level of the neutral system to the vacuum level.

The potential of the system with respect to the standard hydrogen electrode (SHE) can be converted from U_{vac} as:

$$U_{SHE} + \Delta U_{SHE} = U_{vac} \tag{10}$$

with the IUPAC recommended value of $\Delta U_{SHE} = 4.44$ V.

All the calculations in this work were performed with the VASP code[42] and further details are provided in the Supporting Information (SI) section 1.

In a first step, we show that, at the DFT level (exemplified using the PBE functional here), the energetic approach developed here is equivalent to the commonly used SCF ap-

proach. Here we consider a 5 layer slab exposing the 1×1 Cu(100) facet with CO adsorbed on the atop site. As shown in Fig. 1 (a), the Fermi level values obtained using these two different approaches agree excellently with each other. Consequently, the quadratic relationship between the electronic free energy G and the potential U, and further the adsorption energy, are found to agree very well for these two approaches. Differences in the adsorption energy over the potential range considered here, -1 to 0 V vs SHE, is smaller than 2 meV. The Fermi level and G(U) parabola comparison between the two approaches for the bare Cu(100) facet is provided in the SI section 2.

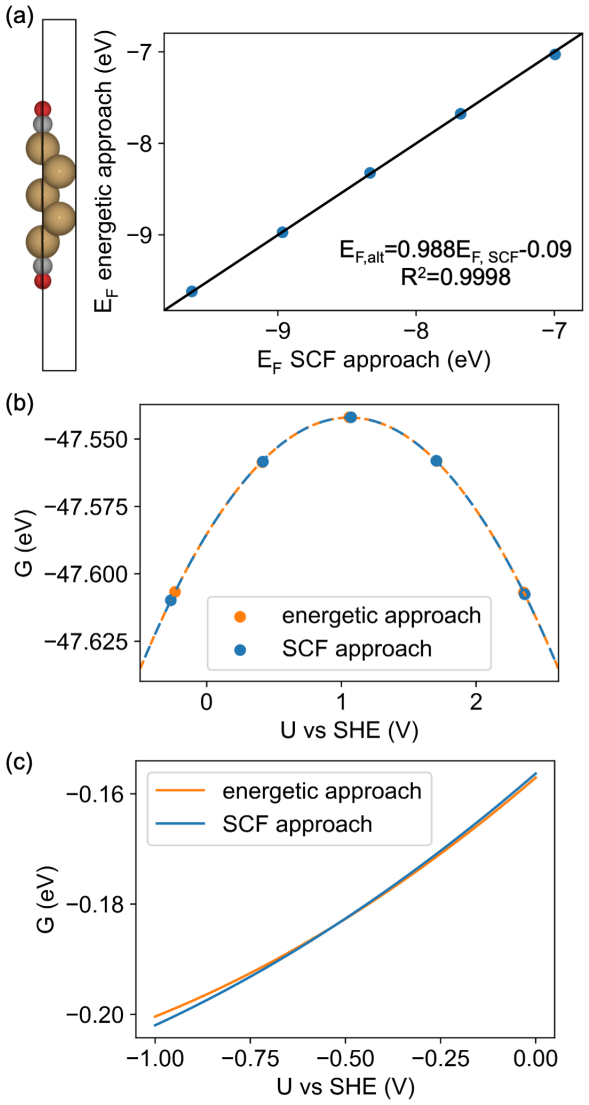

Figure 1: (a) Fermi level E_F values at the GGA level obtained using the energetic approach developed in this work compared to the ones taken directly from the SCF electronic structure. The blue dots are the data and the black line indicates a perfect match. The corresponding unit cell structure, a 5 layer slab exposing 1×1 Cu(100) facet with CO adsorbed on the atop site, is shown. Cu atoms are shown as brown, O atoms red, and C atoms grey. (b) The potential dependent free energy of the adsorbed CO system calculated using the energetic approach compared to the results using the SCF approach. Dots are data points and dashed lines are the fitted parabola. (c) The potential dependent adsorption energy of CO in the atop site calculated using the energetic approach compared to the results using the SCF approach.

Having this energetic approach validated at the DFT level, the grand canonical treatment can be further applied to the RPA energetics. We considered a series of different metal

facets, the (100), (110), and (111) facets of Cu, Ag, and Au, and test whether the quadratic relationship established in Eq. 9 is correctly captured. Indeed, we find that the expected quadratic relationship is achieved for each of these facets. As an example, the quadratic relationship of the Cu(100) facet is shown in Fig. 2 (a). The quality of the quadratic relationship is indicated by the good match of PZC estimated from the parabola and the one of the neutral system, i.e., the data point at the apex. It is worth mentioning that using the Fermi level values of the underlying PBE orbitals cannot give the expected behavior around the PZC, as shown in the SI section 3. The quadratic relationship around the PZC indicates that the correct values of the Fermi level are achieved and thus validates our energetic approach. The comparison between the GC-RPA and experimental PZC values is shown in Fig. 2 (b).

Using the least square fitting with a fixed slope of 1, we obtained a ΔU_{SHE}^{pred}=5.31 V. Compared to the IUPAC recommended value, 4.44 V, RPA seems to overestimate PZC values. The magnitude of the overestimation is, however, unclear, considering that experiments show a large error bar[44,45] ($\pm$0.5 V) and that a recent report[46] indicates that the work function of the SHE might be significantly higher. Moreover, a certain extent of overestimation is not entirely surprising, as it has been shown that non-self-consistent RPA (RPA@TPSS) overestimates the ionization potentials for molecules.[47] As we mentioned previously, the PZC, which is directly linked with the work function, serves as an analog to the ionization potential: these energies describe the process of taking one electron from the HOMO or Fermi level to the vacuum level, in the molecular or periodic systems, respectively. It is worth mentioning that the accuracy of molecular properties using RPA methods can be further improved when self-consistent approaches are used[48] and the work function overestimation here may be mitigated as well.

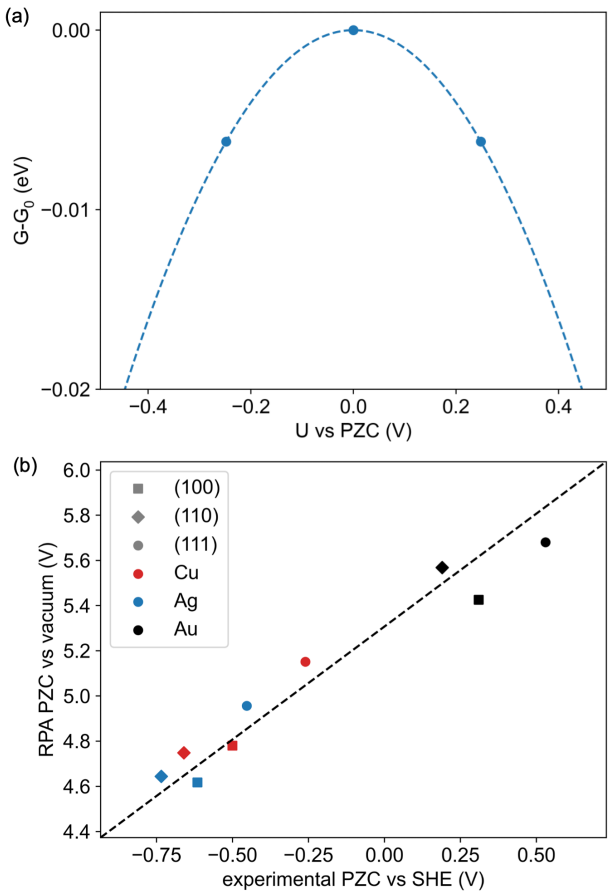

Figure 2: (a) The quadratic relationship between the GC-RPA electronic free energy and the potential of the system of a Cu(100) facet model. (b) Comparison between the computed RPA and the experimental potential of zero charge (PZC) values with respect to the standard hydrogen electrode (SHE). The dashed line is a fit of $U_{vac}^{pred} = U_{SHE}^{exp} + \Delta U_{SHE}^{pred}$ to determine the theoretical potential of the SHE versus vacuum, here found to be 5.31 V at the GC-RPA level. The experimental values are taken from literature and the detailed values are listed in the SI section 4.

We further applied this method to the potential dependent adsorption of a CO molecule on the Cu(100) facet comparing the top and hollow adsorption site, as shown in Fig. 3. A 5 layer slab exposing a $\sqrt{2} \times \sqrt{2}$ Cu(100) facet was considered, as this corresponds to the experimentally observed 0.5 monolayer coverage. Experimentally, at -0.9 V vs SHE, CO adsorption in the atop site is still preferred (indicated by the frequencies over 2000 cm^{-1}), forming a $\sqrt{2} \times \sqrt{2}$ pattern. The IUPAC recommended ΔU_{SHE}^{pred}=4.44 V was used here for all the methods and the version with fitted ΔU_{SHE}^{pred}=5.31 V for RPA is provided in the SI

section 5. The PBE energetics predict that the hollow site for CO is more stable than the top site for potentials lower than -0.32 V, being consistent with the over-stabilization of the hollow site in the constant charge model. The RPBE and RPA energetics predict the crossover to happen at -1.41 and -1.43 V, respectively, which are both more negative than the experimental probed region and consistent with the experimentally observed atop site adsorption at -0.9 V versus SHE.

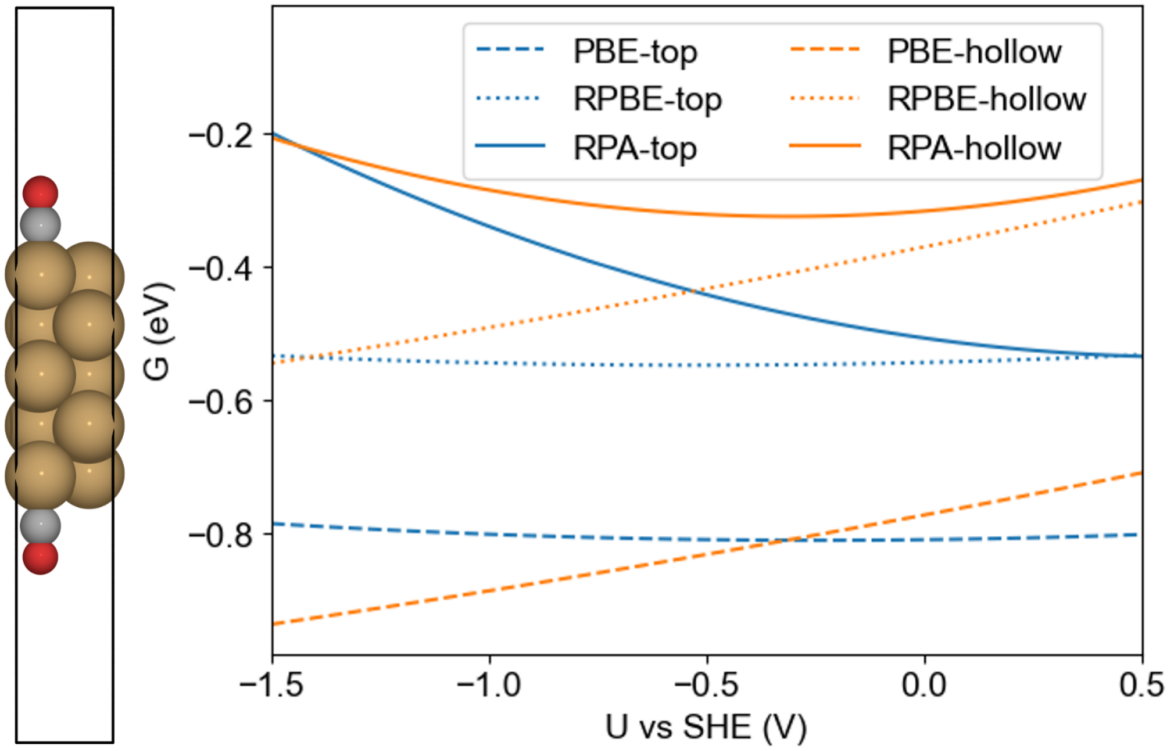

Figure 3: Potential dependent energetics of CO adsorbed at top (blue) and hollow (orange) site, using the grand canonical treatment with the PBE (dashed line), RPBE functionals (dotted line), and RPA (solid line). The experimentally inferred $\sqrt{2} \times \sqrt{2}$ structure, where half of atop sites are covered by CO, is shown. Cu atoms are shown as brown, O atoms red, and C atoms grey.

However, a correct description of potential dependent energetics involves more than just the crossing point. Both GGA functionals predict an almost linear dependence of the adsorption energy with respect to the potential for atop and hollow sites. The slopes are close to zero for the CO adsorption at the atop site and positive (∼0.2 eV/V) for the hollow

site. The linear relationship indicates that the capacitance, C, in the quadratic relationship (Eq. 9) is unchanged before and after the adsorption. Interestingly, at the RPA level, larger curvatures are obtained for both the atop and hollow site adsorption compared to the GGA results, indicating a larger change in double layer capacitance after adsorption, which is consistent with the experimental observation that the double layer capacitance is modified by adsorbates.[49–51] Moreover, it is worth mentioning that the slope of the adsorption relationships indicates the direction of the charge flow upon adsorption:[13] a positive (negative) slope indicates that charge is injected into (depleted from) the surface after the adsorption, i.e., the system gets reduced (oxidized). The reduction of hollow site adsorption at the GGA level is, however, concerning, as experimentally it has been shown that the addition of a cation, which effectively reduces the adsorbates, will steer the selectivity towards C_2 products.[52] If the reduction predicted by the RPBE functional for the hollow site adsorption happens, the dimerization of CO adsorbed at the metastable hollow site could take place without the presence of cation. In contrast, at the RPA level, the predicted negative slopes, i.e., the depletion of electrons, for both the CO adsorption at the atop and hollow sites are in line with the observed improvement when cations are present. These facts show that at the GGA level, the improvement of the potential dependent stability using the RPBE functional compared to the PBE functional is mostly a vertical shift of the potential dependent adsorption energies. More importantly, the other aspects of the potential dependent energetics, including the curvature reflecting the capacitance and the slope reflecting the charge injection behavior, are still inconsistent with experimental evidences, and can be improved using the GC-RPA energetics.

In conclusion, we present an "energetic" grand-canonical approach for electrocatalytic interface simulations, which can be applied to any electronic structure method that produces total energies. Specifically, we here have introduced the grand canonical treatment of electrons within the RPA framework, here called GC-RPA. We applied this method to three facets of Cu, Ag, and Au and found the expected quadratic behavior around the PZC,

and a good reproduction of the experimental PZC values. We further applied this method to the potential dependent CO adsorption on the Cu(100) facet. The grand canonical RPA energetics gives qualitative and quantitative differences compared to the GGA results. Compared to RPBE, which improves upon PBE by shifting energies vertically, GC-RPA predicts larger curvatures, which indicate changes in the capacitance, and different slopes which show a different charge injection mechanism upon CO adsorption. Both observations are more consistent with the experimental evidences compared to the GGA results. We expect this development to pave the way to further electrochemical applications of RPA, and more generally, post-HF methods without a self-consistent electronic structure.

Supporting Information

Supporting Information: Computational details; comparison between the SCF and the energetic approaches of the Cu(100) facet at the PBE level; the grand canonical RPA energetics using the Fermi level of the underlying DFT orbitals; experimental PZC values; potential dependent RPA energetics of CO adsorption using the fitted potential of SHE

Acknowledgement

The calculations were performed on the Hoffman2 cluster at UCLA Institute for Digital Research and Education (IDRE) and the Extreme Science and Engineering Discovery Environment (XSEDE),[53] which is supported by National Science Foundation grant number ACI-1548562, through allocation TG-CHE170060. F. Göltl acknowledges support from the College of Agriculture and Life Science at the University of Arizona. S. N. Steinmann thanks the SYSPROD project and AXELERA Pôle de Compétitivité for financial support (PSMN Data Center). P. Sautet acknowledges the support from National Science Foundation CBET grant 2103116.

References

(1) Seh, Z. W.; Kibsgaard, J.; Dickens, C. F.; Chorkendorff, I.; Nørskov, J. K.; Jaramillo, T. F. Combining theory and experiment in electrocatalysis: Insights into materials design. *Science* **2017**, *355*, eaad4998.

(2) Jiao, Y.; Zheng, Y.; Jaroniec, M.; Qiao, S. Z. Design of electrocatalysts for oxygen-and hydrogen-involving energy conversion reactions. *Chem. Soc. Rev.* **2015**, *44*, 2060–2086.

(3) Gasteiger, H. A.; Marković, N. M. Just a dream—or future reality? *Science* **2009**, *324*, 48–49.

(4) Costentin, C.; Robert, M.; Savéant, J.-M. Catalysis of the electrochemical reduction of carbon dioxide. *Chem. Soc. Rev.* **2013**, *42*, 2423–2436.

(5) Mikkelsen, M.; Jørgensen, M.; Krebs, F. C. The teraton challenge. A review of fixation and transformation of carbon dioxide. *Energy Environ. Sci.* **2010**, *3*, 43–81.

(6) Mathew, K.; Kolluru, V. C.; Mula, S.; Steinmann, S. N.; Hennig, R. G. Implicit self-consistent electrolyte model in plane-wave density-functional theory. *J. Chem. Phys.* **2019**, *151*, 234101.

(7) Xiao, H.; Cheng, T.; Goddard, W. A.; Sundararaman, R. Mechanistic explanation of the pH dependence and onset potentials for hydrocarbon products from electrochemical reduction of CO on Cu (111). *J. Am. Chem. Soc.* **2016**, *138*, 483–486.

(8) Goodpaster, J. D.; Bell, A. T.; Head-Gordon, M. Identification of possible pathways for C–C bond formation during electrochemical reduction of CO2: New theoretical insights from an improved electrochemical model. *J. Phys. Chem. Lett.* **2016**, *7*, 1471–1477.

(9) Shang, R.; Steinmann, S. N.; Xu, B.-Q.; Sautet, P. Mononuclear Fe in N-doped carbon: Computational elucidation of active sites for electrochemical oxygen reduction and oxygen evolution reactions. *Catal. Sci. Technol.* **2020**, *10*, 1006–1014.

(10) Kohn, W.; Sham, L. Self-consistent equations including exchange and correlation effects. *Phys. Rev.* **1965**, *140*, A1133–A1138.

(11) Hohenberg, P.; Kohn, W. Inhomogeneous electron gas. *Phys. Rev.* **1964**, *136*, B864–B871.

(12) Sundararaman, R.; Goddard, W. A. The charge-asymmetric nonlocally determined local-electric (CANDLE) solvation model. *J. Chem. Phys.* **2015**, *142*, 064107.

(13) Steinmann, S. N.; Michel, C.; Schwiedernoch, R.; Sautet, P. Impacts of electrode potentials and solvents on the electroreduction of CO2: A comparison of theoretical approaches. *Phys. Chem. Chem. Phys.* **2015**, *17*, 13949–13963.

(14) Smidstrup, S.; Stradi, D.; Wellendorff, J.; Khomyakov, P. A.; Vej-Hansen, U. G.; Lee, M.-E.; Ghosh, T.; Jónsson, E.; Jónsson, H.; Stokbro, K. First-principles Green's-function method for surface calculations: A pseudopotential localized basis set approach. *Phys. Rev. B* **2017**, *96*, 195309.

(15) Danielewicz, P. Quantum theory of nonequilibrium processes, I. *Ann. Phys-new. York.* **1984**, *152*, 239–304.

(16) Ohto, T.; Rungger, I.; Yamashita, K.; Nakamura, H.; Sanvito, S. Ab initio theory for current-induced molecular switching: Melamine on Cu(001). *Phys. Rev. B* **2013**, *87*, 205439.

(17) Pedroza, L. S.; Brandimarte, P.; Rocha, A. R.; Fernández-Serra, M.-V. Bias-dependent local structure of water molecules at a metallic interface. *Chem. Sci.* **2018**, *9*, 62–69.

(18) Gajdoš, M.; Eichler, A.; Hafner, J. CO adsorption on close-packed transition and noble metal surfaces: Trends from ab initio calculations. *J. Phys. Condens. Matter* **2004**, *16*, 1141.

(19) Feibelman, P. J.; Hammer, B.; Nørskov, J.; Wagner, F.; Scheffler, M.; Stumpf, R.; Watwe, R.; Dumesic, J. The CO/Pt(111) puzzle. *J. Phys. Chem. B* **2000**, *105*, 4018–4025.

(20) Kresse, G.; Gil, A.; Sautet, P. Significance of single-electron energies for the description of CO on Pt(111). *Phys. Rev. B* **2003**, *68*, 073401.

(21) Nozières, P.; Pines, D. Correlation energy of a free electron gas. *Phys. Rev.* **1958**, *111*, 442–454.

(22) Harl, J.; Kresse, G. Cohesive energy curves for noble gas solids calculated by adiabatic connection fluctuation-dissipation theory. *Phys. Rev. B* **2008**, *77*, 045136.

(23) Gunnarsson, O.; Lundqvist, B. Exchange and correlation in atoms, molecules, and solids by the spin-density-functional formalism. *Phys. Rev. B* **1976**, *13*, 4274–4298.

(24) Langreth, D. C.; Perdew, J. P. Exchange-correlation energy of a metallic surface: Wave-vector analysis. *Phys. Rev. B* **1977**, *15*, 2884–2901.

(25) Schimka, L.; Harl, J.; Stroppa, A.; Grüneis, A.; Marsman, M.; Mittendorfer, F.; Kresse, G. Accurate surface and adsorption energies from many-body perturbation theory. *Nature Mater* **2010**, *9*, 741–744.

(26) Wei, Z.; Göltl, F.; Sautet, P. Diffusion barriers for carbon monoxide on the Cu(001) surface using many-body perturbation theory and various density functionals. *J. Chem. Theory Comput.* **2021**, *17*, 7862–7872.

(27) Hori, Y.; Takahashi, R.; Yoshinami, Y.; Murata, A. Electrochemical reduction of CO at a copper electrode. *J. Phys. Chem. B* **1997**, *101*, 7075–7081.

(28) Schouten, K. J. P.; Qin, Z.; Pérez Gallent, E.; Koper, M. T. Two pathways for the formation of ethylene in CO reduction on single-crystal copper electrodes. *J. Am. Chem. Soc.* **2012**, *134*, 9864–9867.

(29) Schmidt, P. S.; Thygesen, K. S. Benchmark database of transition metal surface and adsorption energies from many-body perturbation theory. *J. Phys. Chem. C* **2018**, *122*, 4381–4390.

(30) Foster, M. E.; Wong, B. M. Nonempirically tuned range-separated DFT accurately predicts both fundamental and excitation gaps in DNA and RNA nucleobases. *J. Chem. Theory Comput.* **2012**, *8*, 2682–2687.

(31) Ma, H.; Govoni, M.; Gygi, F.; Galli, G. A finite-field approach for GW calculations beyond the random phase approximation. *J. Chem. Theory. Comput.* **2018**, *15*, 154–164.

(32) Brunin, G.; Ricci, F.; Ha, V.-A.; Rignanese, G.-M.; Hautier, G. Transparent conducting materials discovery using high-throughput computing. *npj Comput. Mater.* **2019**, *5*, 1–13.

(33) Zhou, Q.; Liu, Z.-F.; Marks, T. J.; Darancet, P. Range-separated hybrid functionals for mixed dimensional heterojunctions: Application to phthalocyanines/MoS2. *APL Mater.* **2021**, *9*, 121112.

(34) Perdew, J. P.; Burke, K.; Ernzerhof, M. Generalized gradient approximation made simple. *Phys. Rev. Lett.* **1996**, *77*, 3865–3868.

(35) Hammer, B.; Hansen, L.; Nørskov, J. Improved adsorption energetics within density-functional theory using revised Perdew-Burke-Ernzerhof functionals. *Phys. Rev. B* **1999**, *59*, 7413–7421.

(36) Harl, J.; Schimka, L.; Kresse, G. Assessing the quality of the random phase approximation for lattice constants and atomization energies of solids. *Phys. Rev. B* **2010**, *81*, 115126.

(37) Yang, W.; Mori-Sánchez, P.; Cohen, A. J. Extension of many-body theory and approximate density functionals to fractional charges and fractional spins. *J. Chem. Phys.* **2013**, *139*, 104114.

(38) Langreth, D.; Perdew, J. The exchange-correlation energy of a metallic surface. *Solid State Commun.* **1975**, *17*, 1425–1429.

(39) Niquet, Y.; Fuchs, M.; Gonze, X. Exchange-correlation potentials in the adiabatic connection fluctuation-dissipation framework. *Phys. Rev. A* **2003**, *68*, 032507.

(40) Dahlen, N. E.; van Leeuwen, R.; von Barth, U. Variational energy functionals of the Green function and of the density tested on molecules. *Phys. Rev. A* **2006**, *73*, 012511.

(41) Mathew, K.; Sundararaman, R.; Letchworth-Weaver, K.; Arias, T.; Hennig, R. G. Implicit solvation model for density-functional study of nanocrystal surfaces and reaction pathways. *J. Chem. Phys.* **2014**, *140*, 084106.

(42) Kresse, G.; Hafner, J. Ab initio molecular dynamics for liquid metals. *Phys. Rev. B* **1993**, *47*, 558–561.

(43) Steinmann, S. N.; Sautet, P. Assessing a first-principles model of an electrochemical interface by comparison with experiment. *J. Phys. Chem. C* **2016**, *120*, 5619–5623.

(44) Trasatti, S. Interfacial behaviour of non-aqueous solvents. *Electrochim. Acta* **1987**, *32*, 843–850.

(45) Fawcett, W. R. The ionic work function and its role in estimating absolute electrode potentials. *Langmuir* **2008**, *24*, 9868–9875.

(46) Haruyama, J.; Ikeshoji, T.; Otani, M. Electrode potential from density functional theory calculations combined with implicit solvation theory. *Phys. Rev. Materials* **2018**, *2*, 095801.

(47) Eshuis, H.; Bates, J. E.; Furche, F. Electron correlation methods based on the random phase approximation. *Theor Chem Acc* **2012**, *131*, 1–18.

(48) Yu, J. M.; Nguyen, B. D.; Tsai, J.; Hernandez, D. J.; Furche, F. Selfconsistent random phase approximation methods. *J. Chem. Phys.* **2021**, *155*, 040902.

(49) Pajkossy, T.; Kolb, D. Double layer capacitance of Pt(111) single crystal electrodes. *Electrochim. Acta* **2001**, *46*, 3063–3071.

(50) Hansen, R. S.; Minturn, R. E.; Hickson, D. A. The inference of adsorption from differential double-layer capacitance measurements. *J. Phys. Chem.* **1956**, *60*, 1185–1189.

(51) Hansen, R. S.; Kelsh, D. J.; Grantham, D. The inference of adsorption from differential double layer capacitance measurements. II. Dependence of surface charge density on organic nonelectrolyte surface excess. *J. Phys. Chem.* **1963**, *67*, 2316–2326.

(52) Pérez-Gallent, E.; Marcandalli, G.; Figueiredo, M. C.; Calle-Vallejo, F.; Koper, M. T. Structure- and potential-dependent cation effects on CO reduction at copper single-crystal electrodes. *J. Am. Chem. Soc.* **2017**, *139*, 16412–16419.

(53) Towns, J.; Cockerill, T.; Dahan, M.; Foster, I.; Gaither, K.; Grimshaw, A.; Hazlewood, V.; Lathrop, S.; Lifka, D.; Peterson, G. D.; Roskies, R.; Scott, J. R.; Wilkins-Diehr, N. XSEDE: accelerating scientific discovery. *Comput. Sci. Eng.* **2014**, *16*, 62–74.

Graphical TOC Entry